



Article

Effects of Micro-Shot Peening on the Stress Corrosion Cracking of Austenitic Stainless Steel Welds

Chia-Ying Kang ¹, Tai-Cheng Chen ²  and Leu-Wen Tsay ^{1,*} ¹ Department of Optoelectronics and Materials Technology, National Taiwan Ocean University, Keelung 20224, Taiwan² Nuclear Fuels and Materials Division, Institute of Nuclear Energy Research, Taoyuan 32546, Taiwan

* Correspondence: b0186@mail.ntou.edu.tw; Tel.: +886-2-24622192 (ext. 6405)

Abstract: Micro-shot peening on AISI 304 and 316 stainless steel (SS) laser welds was performed to evaluate its effect on the susceptibility to stress corrosion cracking (SCC) in a salt spray containing 10% NaCl at 80 °C. The cracking susceptibility of the welds was disclosed by testing U-bend specimens in a salt spray. Micro-shot peening caused an intense but narrow deformed layer with a nanocrystal structure and residual compressive stress. Austenite to martensite transformation occurred heavily on the top surface of the micro-shot peened welds. SCC microcracks were more likely to be initiated at the fusion boundary (FB) of the non-peened welds. However, fine pits were formed more easily on the micro-shot peened 304 fusion zone (FZ), which was attributed to the extensive formation of strain-induced martensite. The nanogained structure and induced residual compressive stress in the micro-shot peened layer suppressed microcrack initiation in the 304 and 316 welds in a salt spray. Compared with the other zones in the welds in a salt spray, the high local strain at the FB was the cause of the high cracking susceptibility and could be mitigated by the micro-shot peening treatment.

Keywords: stainless steel weld; micro-shot peening; stress corrosion cracking; residual stress; nanogained structure



Citation: Kang, C.-Y.; Chen, T.-C.; Tsay, L.-W. Effects of Micro-Shot Peening on the Stress Corrosion Cracking of Austenitic Stainless Steel Welds. *Metals* **2023**, *13*, 69. <https://doi.org/10.3390/met13010069>

Academic Editor: Koji Takahashi

Received: 4 December 2022

Revised: 23 December 2022

Accepted: 23 December 2022

Published: 26 December 2022



Copyright: © 2022 by the authors. Licensee MDPI, Basel, Switzerland. This article is an open access article distributed under the terms and conditions of the Creative Commons Attribution (CC BY) license (<https://creativecommons.org/licenses/by/4.0/>).

1. Introduction

Surface modification processes are considered to provide superior surface properties to enhance the wear, corrosion and fatigue resistance of structural components. Among the various surface treatments, shot-peening is widely applied in industry because of its easy control, industrial adaptability and cost effectiveness. Shot peening is reported to cause grain refinement and nano-crystallization in the surface and subsurface area of austenitic stainless steels [1–6], which are expected to have noticeable mechanical, physical and chemical characteristics. Moreover, shot peening has many advantages on material properties, including tribology [7,8], biocompatibility [9], anti-wear [10] and fatigue [11–14]. Although the increase in surface roughness after shot-peening may deteriorate the fatigue strength, the introduced residual compressive stress is able to increase the fatigue strength/life of 304 and/or 316 stainless steels (SSs) [15–17]. Strain-induced martensitic transformation may occur in metastable austenitic SSs during straining [18–20] and, in a severely shot-peened layer, austenite to martensite transformation may also occur [2,5]. It is reported that huge numbers of dislocations are found in the lath martensite within the nano-grained region [2]. Moreover, the martensite morphology will change from lath to cell type because martensite laths are broken up by the high strain rate and multi-directional impacts of the shot at the topmost surface [2].

Compared with the conventional shot peening, micro-shot peening uses fine shot balls with particle sizes of less than 100 µm to bombard the substrate surface [21,22]. With the use of fine particles for shot peening, the surface roughness can be reduced [21,22] and high residual compressive stress is introduced, compared with conventional shot peening. Another important issue with shot-peened austenitic SSs is their corrosion resistance. The

corrosion resistance of shot-peened 304 SS is reported to be improved with decreasing surface roughness, as the practical area for corrosion per unit area increases with increasing surface roughness [23]. Grain refinement and residual compressive stress enhance the corrosion resistance, but the high surface roughness and induced martensite decrease the corrosion resistance of shot-peened 304 SS [24]. Moreover, ultrasonic and accelerated shot-peening increase the corrosion resistance in a 3.5% NaCl solution of 316 [10] and 316 LN [25] SSs, respectively. Regarding the stress corrosion cracking (SCC) of 304 and 316 SSs, shot-peening is reported to suppress crack initiation and propagation in chloride-containing solutions [16,26,27]. The compressive residual stress in the shot-peened layer inhibits the occurrence of SCC by preventing the fracture of the surface oxide film [26].

Pipelines and reactors made of conventionally welded austenitic SS are sensitive to SCC [28,29]. The presence of high tensile residual stress in the weld metal (WM) and heat-affected zone (HAZ) of the 304 SS weld assists the occurrence of SCC [30]. The effect of micro-shot peening on the SCC susceptibility of the SS welds is less disclosed in the open literatures; therefore, the aim of this study is to evaluate the role of micro-shot peening on the SCC behavior of the 304 and 316 welds. In this work, 304 and 316 laser welds were subjected to shot peening with fine particles. The surface deformation introduced by micro-shot peening was determined by the Almen intensity. The change in surface roughness before and after micro-shot peening was examined with a 3D contour profiler. The crack initiation of the U-bend samples was inspected with a scanning electron microscope (SEM). The induced phase transformation and grain-refined zone were identified by electron backscatter diffraction (EBSD). The effects of the refined microstructure and induced residual stress of the micro-shot peened samples were investigated and correlated with the SCC cracking susceptibility of the tested samples.

2. Materials and Experimental Procedures

AISI 304 and 316 steel plates with a thickness of 2.0 mm in the mill-annealed condition were used in this study. The microstructure of the mill-annealed 304 and 316 plates consisted of a granular austenite matrix with few twins inside. The steel plates were welded in a direction normal to the rolling direction. A 5 kW CO₂ laser in keyhole mode was utilized for autogenous bead-on-plate welding of the steel plates in full penetration. The welding variables included a laser power of 2.4 kW and a travel speed of 1200 mm/min. Figure 1 shows the schematic illustration of the weldment along with the normal direction (ND), rolling direction (RD) and transverse direction (TD) of the sample. The 304 and 316 plates were ground with 2000 grit sandpaper before U-bending. The weld reinforcement was removed progressively by grinding with SiC sandpapers. Some of the U-bend samples were micro-shot peened with Fe-based amorphous particles of 50–100 µm in size under 200% surface coverage. The micro-shot peening intensity determined by the height of the N-type Almen specimen was 0.169 mm. Accurate surface metrology of the micro-shot peened specimens was carried out by using a ContourGT-K 3D optical profiler (Bruker, Billerica, MA, USA) providing non-contact surface measurements. An MVK-G1500 Vickers micro-hardness tester (Mitutoyo, Kawasaki, Japan) was used to determine the hardness in distinct zones of a weld under the load of 300 gf for 15 s. The ferrite contents of different specimens were measured with a Fischer FMP30 ferrite scope (Helmut Fischer, Sindelfingen, Germany) and expressed in the ferrite number (FN). For ease in measuring the ferrite content of the fusion zone (FZ), the weld reinforcement was ground with sandpaper, which could cause an increase in FN. However, the trend of the change in ferrite content of the FZ was still meaningful.

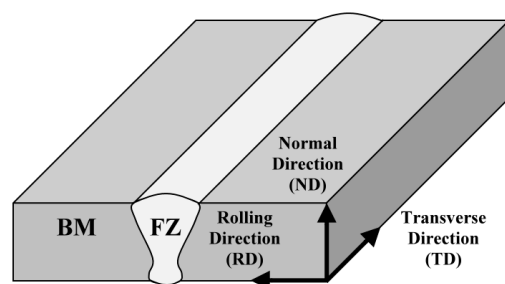


Figure 1. Schematic illustration showing the normal direction (ND), rolling direction (RD) and transverse direction (TD) of the weldment.

In the case of the SCC tests, U-bend samples with original dimensions of 10 mm (W) \times 120 mm (L) \times 2 mm (T) were applied for testing in a salt spray containing 10% NaCl at 80 °C. The augmented strain ε generated at the outer surface of the bent specimen was calculated according to the following equation:

$$\varepsilon (\%) = \frac{t}{2R} \times 100 \quad (1)$$

where t is the sample thickness and R is the radius of the die block. U-bend samples with a 10% augmented strain were imposed in the test using a die block of 10 mm in radius. To inspect the change in surface condition of the U-bend sample, the tested sample was periodically removed from the salt spray chamber and examined with an SZ-ST5 stereo-microscope (Olympus, Tokyo, Japan) at 30 \times magnification. The SCC tests of various samples were terminated after 4 weeks (672 h) in a salt spray. After the testing, the U-bend samples were sectioned into small samples and subjected to metallographic preparation for further investigation.

The μ -X360s (Pulstec, Hamamatsu, Japan), a residual stress analyzer, was applied to determine the distributions of residual stress in as-welded samples with or without micro-shot peening. The stress-measured area included the full FZ and a portion of the HAZ. The μ -X360s X-ray source provided Cr target K α radiation (wavelength 2.291 Å) at an X-ray tube voltage of 30 kV with 1.5 mA current. The μ -X360s device for measuring residual stress is based on the $\cos \alpha$ method. The distribution of residual stress in the thickness direction was obtained by removing the surface layer of the sample using a Model EP-3 electrochemical polisher (Pulstec, Hamamatsu, Japan). The macro-appearances and surface features of the U-bend specimens after SCC tests were examined with a S-3400 N SEM (Hitachi, Tokyo, Japan). The strain-induced α' -martensite and refined structure of the micro-shot peened layer were inspected by using the EBSD (Oxford Instruments, Abingdon, UK) mapping. Moreover, the strain distribution maps of the tested samples were analyzed by using the HKL Channel 5 software (Oxford Instruments, Abingdon, UK) to process the original data obtained by the EBSD.

3. Results

3.1. Microstructural Observation of the Welds

Figure 2 shows the macro- and microstructures of the laser welds in a cross-sectional view. As shown in Figure 2a,b, the laser weld was in the shape of a wine glass, consisting of solidified columnar grains in the FZ and unequally sized grains in the HAZ and base metal (BM). The microstructures of the BMs of the 304 and 316 SSs were a granular austenite matrix with twins inside. The FZ microstructure of a 304 weld consisted of a skeletal structure with vermicular ferrite (δ ferrite) within the austenite matrix (Figure 2c). By contrast, the FZ of the 316 weld contained cellular dendrites of austenite without any precipitates (Figure 2d). It is reported that the SCC of 304 laser welds in 1 M NaCl + 0.5 M HCl is associated with the preferential dissolution of δ ferrite in the WM, which results in

crack propagation along the dendrite boundaries [31]. Therefore, the presence of δ ferrite in the FZ was expected to lower the SCC resistance of a 304 laser weld.

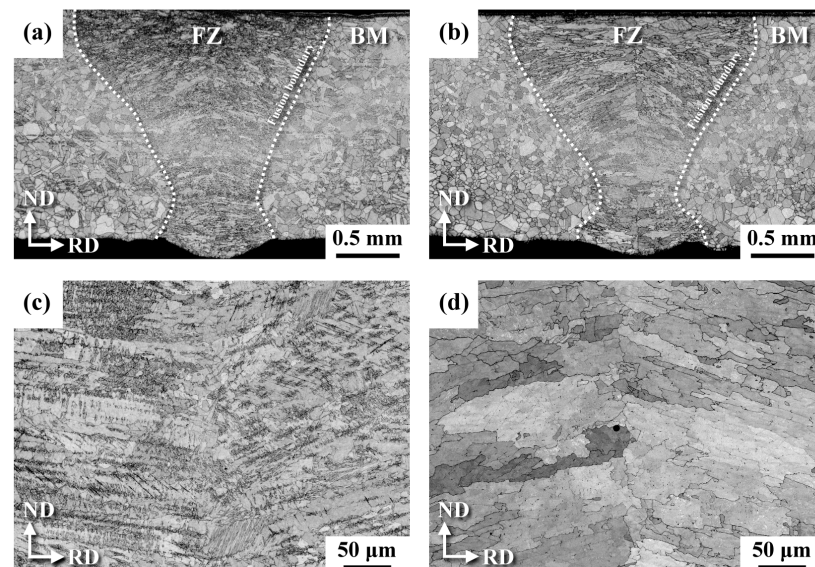


Figure 2. Macro-views of the (a) 304 and (b) 316 laser welds; FZ microstructures of the (c) 304 and (d) 316 welds in a cross-sectional view.

3.2. 3D Contour Profiles of the Ground Substrate and Micro-Shot Peened Samples

Round amorphous particles of 50–100 μm in size were used as the shot balls to bombard the laser welds. The typical feature of a micro-shot peened surface is fine shallow dents of different sizes [21]. The surface roughness values of the tested samples with and without micro-shot peening were determined with an optical profiler. Three-dimensional contour profiles of the ground and micro-shot peened samples are shown in Figure 3 and the surface roughness values of the samples are listed in Table 1. Plastic deformation on the peened surface naturally increased the surface roughness of the micro-shot peened sample. The ground scratches were replaced by fine dents, which were formed due to the impingement of the amorphous shot. The results indicated that the surface roughness values of the 304 and 316 micro-shot peened samples were similar to those of the corresponding substrates. Therefore, a minor increase in surface roughness of the tested samples, which would be less harmful to the corrosion resistance, could be obtained by the use of micro-shot peening.

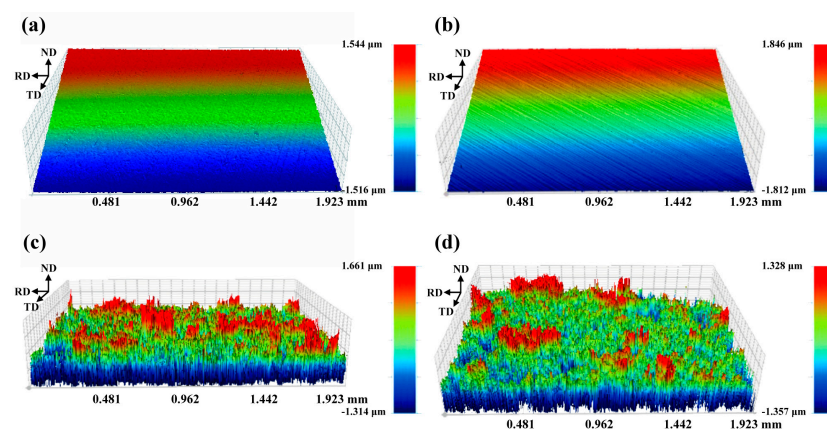


Figure 3. The 3D contour profiles of the (a) ground 304 plate, (b) ground 316 plate, (c) micro-shot peened 304 plate and (d) micro-shot peened 316 plate. The roughness values are listed in Table 1.

Table 1. The roughness values (unit: μm) of ground and micro-shot peened samples measured by a 3D optical profiler.

Specimen	Sa ¹	Sp ²	Sv ³
Ground 304	0.016	0.108	0.205
Ground 316	0.016	0.092	0.459
Micro-shot peened 304	0.209	1.672	1.301
Micro-shot peened 316	0.208	1.305	1.444

¹ Sa—arithmetical mean height of the surface. ² Sp—maximum peak height of the surface. ³ Sv—maximum pit depth of the surface.

3.3. Amount of the Ferromagnetic Phase Determined by Ferrite Scope

The amounts of ferromagnetic phase present in the detected areas of the tested samples, which were determined with a ferrite scope are listed in Table 2. The measured ferromagnetic phase in the tested samples could include different sources, such as the original ferrite in the substrate, induced α' -martensite after straining or the δ ferrite retained in the FZ. The 304 and 316 BMs were both free of the ferrite phase. In the as-welded condition, the FZs of the 304 and 316 welds had ferrite numbers of about 1.76 and 0.54, respectively. The measured ferrite contents confirmed the microstructural observations shown in Figure 2c, i.e., the skeletal structure with δ ferrite in the 304 FZ. As revealed previously [21], micro-shot peening causes intense plastic deformation, which induces austenite to martensite transformation in the thin surface layer of the peened sample. The ferromagnetic phase determined by the ferrite scope has greater validity if the distribution of ferrite in the detected area is uniform. However, a qualitative analysis of the change in ferrite content after micro-shot peening allowed an evaluation of the trend of induced martensitic transformation. The ferrite numbers of the micro-shot peened 304 and 316 substrates were 0.82 and 0.27, respectively, indicating that the 316 SS was more stable and resistant to stress-induced transformation than the 304 SS. After micro-shot peening, the ferrite numbers of the FZs of the 304 and 316 welds increased to 4.41 and 2.10, accordingly. The results indicated that the micro-shot peening had a great influence on assisting the martensitic transformation in the FZ of a 304 weld and that stress-induced transformation was more likely to occur in the FZ of a 304 weld under severe peening, compared with a 316 weld.

Table 2. The ferrite numbers of the tested samples determined by ferrite scope.

Specimen	BM	Micro-Shot Peened BM	FZ	Micro-Shot Peened FZ
304	0.00	0.82 ± 0.25	1.76 ± 0.21	4.41 ± 0.58
316	0.00	0.27 ± 0.12	0.54 ± 0.11	2.10 ± 0.51

3.4. The Micro-Hardness Distributions of the Micro-Shot Peened Welds

The hardness distributions across the FZ of the laser welds are shown in Figure 4. The hardness was measured at 5 and 20 μm from the top surfaces of the welds. Before micro-shot peening, the weld reinforcement was gently removed with SiC sandpaper. The 304 and 316 substrates in the mill-annealed condition had the hardness of about HV 180. The results indicated that the micro-shot peening caused obvious hardening near the outermost surface, regardless of the welds. The FZ also exhibited a higher trend of strain hardening than that of the BM, distinguished by the difference in hardness between them. At the sites 20 μm from the top surfaces of the welds, the FZ and the BM had nearly the same hardness. A significant hardness drop occurred within 20 μm of depth. Thus, micro-shot peening would alter the surface characteristics of the peened sample only to a very shallow depth.

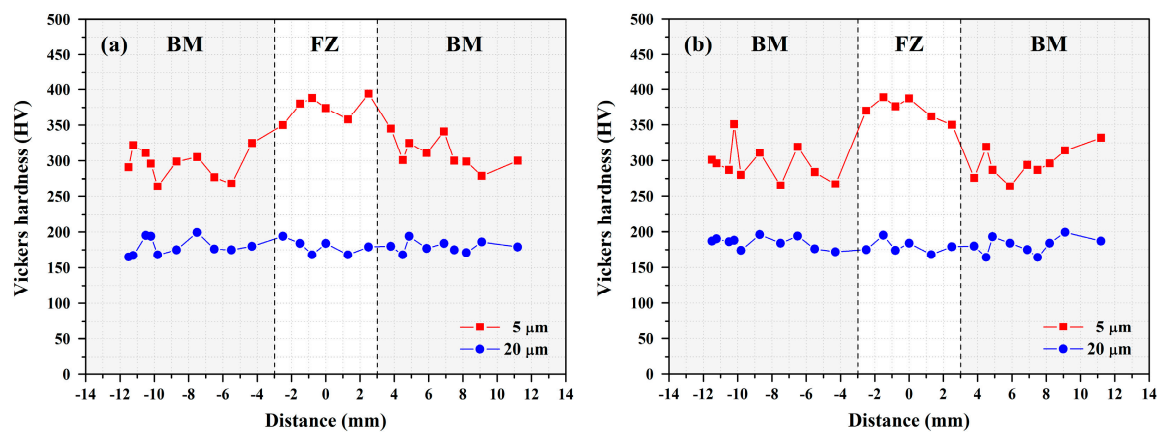


Figure 4. The hardness distributions across the FZs of the micro-shot peened (a) 304 and (b) 316 laser welds at depths of 5 and 20 μm from the top surfaces of the welds.

3.5. EBSD Analysis of the Non-Peened Welds

Figure 5 presents the EBSD analysis showing the outermost microstructures in a cross-sectional view around the fusion boundary (FB) of the U-bend welds without micro-shot peening. The band contrast (BC) maps show the microstructures of 304 and 316 welds (Figure 5a,d). A granular structure with twins inside the grains was observed in the BM sides near the FBs of the two welds (Figure 5a,d). The imposed bending strain introduced the basket-weaved slip bands into the sample, which were associated with the operation of multiple slip systems $\{111\} \langle 110 \rangle$ in the austenitic SSs. Aligned slip lines were clearer in the 304 weld and extended deeply into the interior, relative to those of the 316 weld. The refined grains along the FB of the 304 weld were more likely to be observed, but were found less at the FB of the 316 weld. The fine patches located at the boundaries in the FZ of the 304 weld were mainly associated with the δ ferrite (Figure 5a). In addition, the grain size in the FZ of the 316 weld was coarser than that of the 304 weld. The presence of few δ ferrites in the FZ of the 304 weld could have been the reason for the grain refinement. Moreover, the low energy input of the laser welding restricted the occurrence of grain growth beside the FB as it was hard to distinguish in both welds. Therefore, the HAZ near the FB and the BM had a similar microstructure.

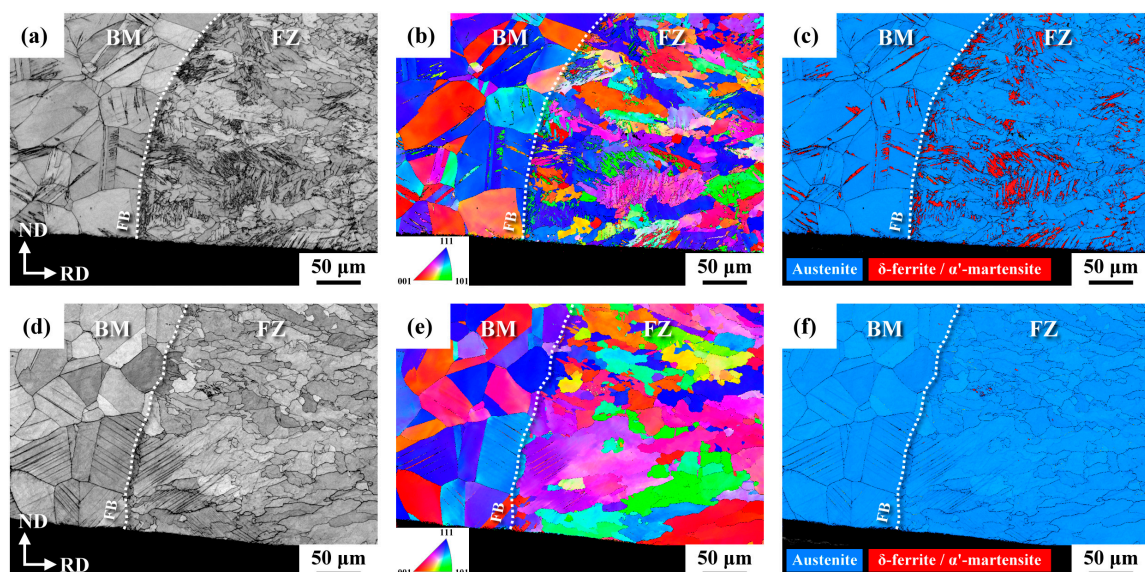


Figure 5. EBSD: (a,d) BC maps, (b,e) IPF maps, (c,f) phase maps of the U-bend samples around FB in cross-sectional view. (a–c) the 304 weld; (d–f) the 316 weld.

Inverse pole figure (IPF) maps (Figure 5b,e) are used to distinguish the grain sizes and orientations of the examined samples. Grains in different orientations were observed in the BM side near the FBs of the two welds. The fine strips present in those two samples were associated with the slip bands caused by the imposed bending strain. Within the FZ, a large patch in the same color confirmed that the solidified structure of the 316 weld was coarser than that of the 304 weld, according to the IPF maps in Figures 5b and 4e. The phase maps revealed the ferromagnetic phase in the 304 weld (Figure 5c) but little in the 316 weld (Figure 5f). The formation of a greater amount of α' -martensite in the BM side of the 304 weld than in that of the 316 weld implied that 316 SS was more resistant than the 304 SS to martensitic transformation under the same applied strain. The high stacking fault energy of the 316 SS relative to that of the 304 SS accounted for the less amount of α' -martensite formed in the former than in the latter [32–35]. It was noticed that the FB of the bent 304 weld consisted of a nearly continuous ferrite phase (Figure 5c), which could be very detrimental to the corrosion and SCC resistance of the 304 weld. Those fine needle-like ferrites present in the FZ of the bent 304 weld could have been the result of stress-induced α' -martensite (Figure 5c).

Figure 6 presents the top microstructures around the FB of the U-bend welds without micro-shot peening, investigated by EBSD. As shown in Figure 6a,d, the BC micrographs displayed a similar microstructure to that in Figure 5a,d. Clearly, the FB of the 304 weld consisted of refined grains, but those fine grains were less common in the FB of the 316 weld. The IPF maps of two different faces of the welds, shown in Figures 5 and 6, also displayed similar microstructures. Based on the phase maps in these two figures, fine needle-like ferrites, likely related to the induced α' -martensite, were more plentiful in the FZ than in the BM adjacent to the FB. This result revealed that, under straining, the solidified FZ was more sensitive to martensitic transformation than the granular substrate. The coarse granular structure in the 304 BM had longer and wider slip bands than those in the FZ (Figure 6c). It was noted that sparse ferrite spots were located along the FB of the 316 weld (Figure 6f). It seemed that, under straining, the FB was highly sensitive to martensitic transformation in both welds and particularly in the 304 weld.

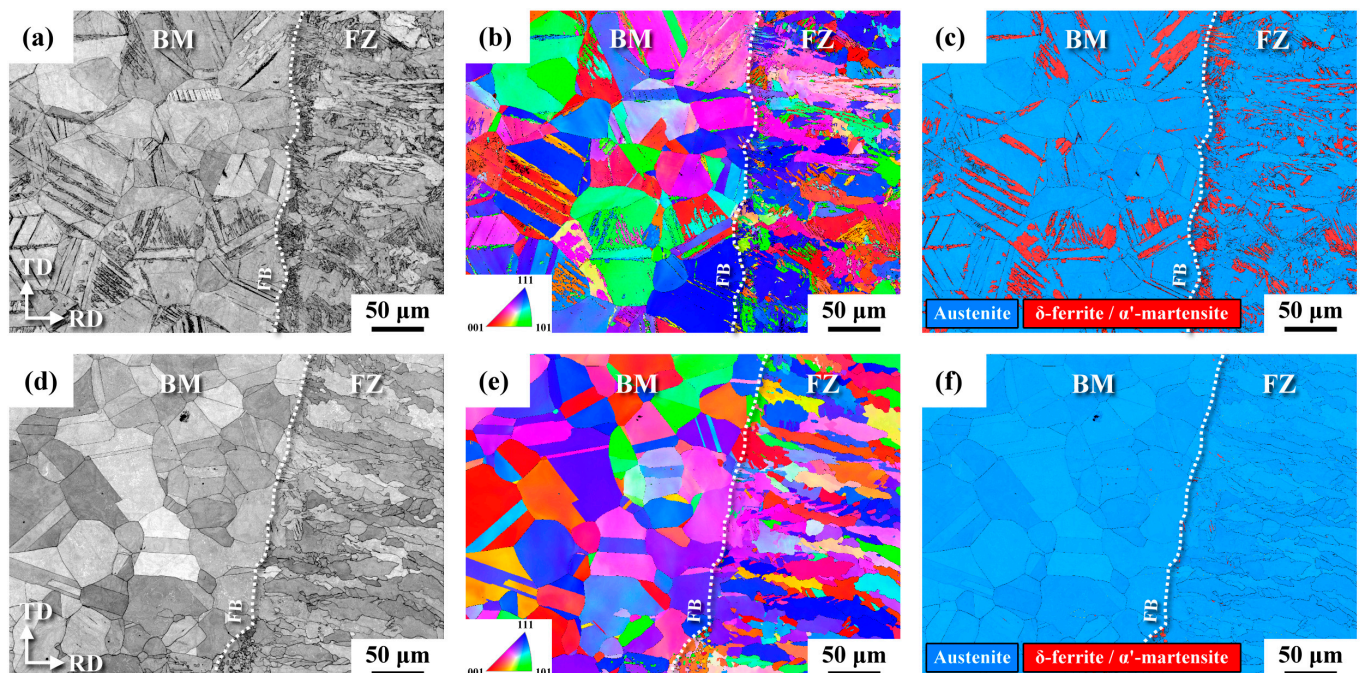


Figure 6. EBSD: (a,d) BC maps, (b,e) IPF maps, (c,f) phase maps of the U-bend samples around the FB in top view. (a–c) the 304 weld; (d–f) the 316 weld.

3.6. EBSD Analysis of the Micro-Shot Peened Welds

The EBSD analysis showing the outermost microstructures of the FZs in the U-bend welds with micro-shot peening are displayed in Figure 7 in a cross-sectional view. The BC micrographs (Figure 7a,d) showed that intense slip lines formed around the peened surface and became sparse about 20 μm from the external surface of the weld. The IPF maps (Figure 7b,e) show that the micro-shot peened layer consisted of extremely fine grains in different orientations. The phase maps confirmed that severe deformation introduced by micro-shot peening caused the intense transformation of austenite to α' -martensite on the outermost surface of the two peened welds (Figure 7c,f). Slim α' -martensite was more common in the 304 weld (Figure 7c) than in the 316 weld (Figure 7f), with increases in distance from the top surface of the peened weld. The ferrite number of the micro-shot peened 304 weld was higher than that of the micro-shot peened 316 weld due to the higher extent of martensitic transformation and the relatively high content of δ ferrite. Moreover, the strain-induced α' -martensite and the fine-grained structure that formed on the peened surface were expected to cause obvious surface-hardening after micro-shot peening.

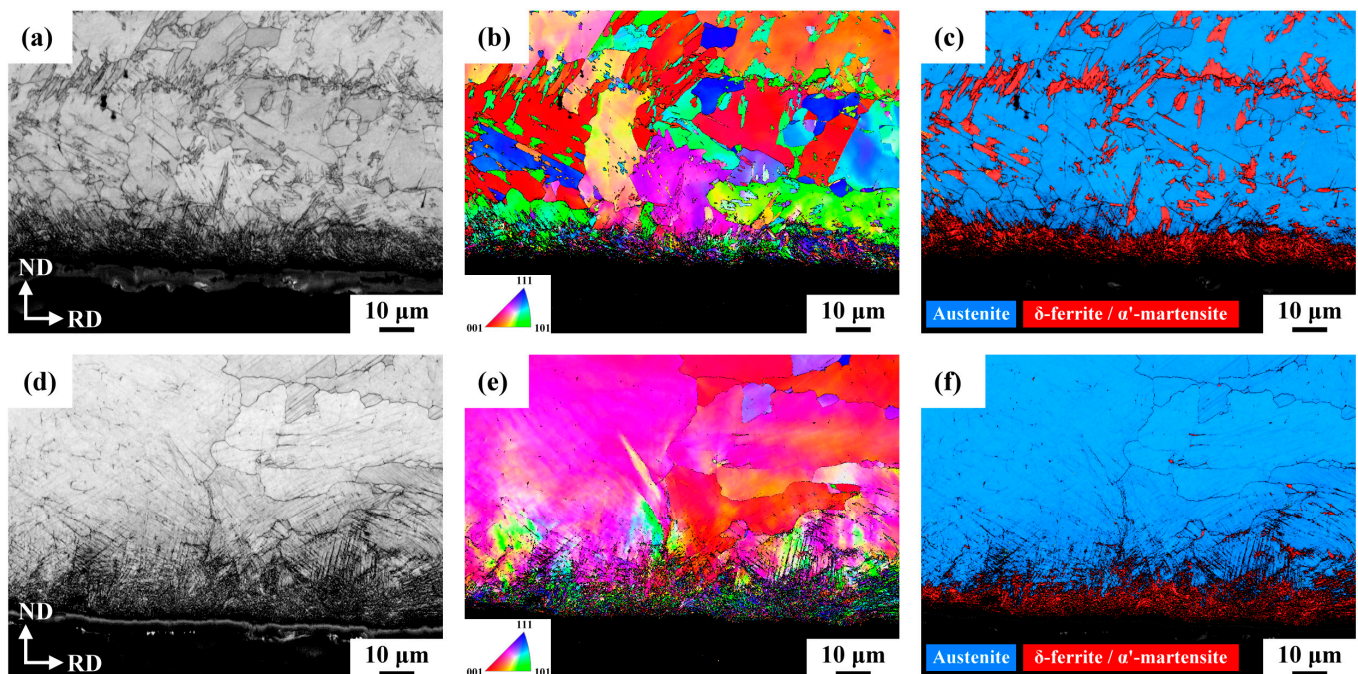


Figure 7. EBSD: (a,d) BC maps, (b,e) IPF maps, (c,f) phase maps of the U-bend samples with micro-shot peening around the FZ in cross-sectional view. (a–c) the 304 weld; (d–f) the 316 weld.

The microstructures around the FB in the U-bend welds with micro-shot peening are presented in Figure 8 in a cross-sectional view. The BC maps and IPF maps of the micro-shot peened sample (Figure 8) were similar to those of the non-peened sample (Figure 5). The phase maps (Figure 8c,f) showed that micro-shot peening caused intense deformation on the top surface around the FBs of the two welds, resulting in the formation dense α' -martensite but only to a finite depth. Thus, the application of intense micro-shot peening in distinct zones of the austenitic SS welds was expected to cause an obvious change in the surface microstructure of the welds.

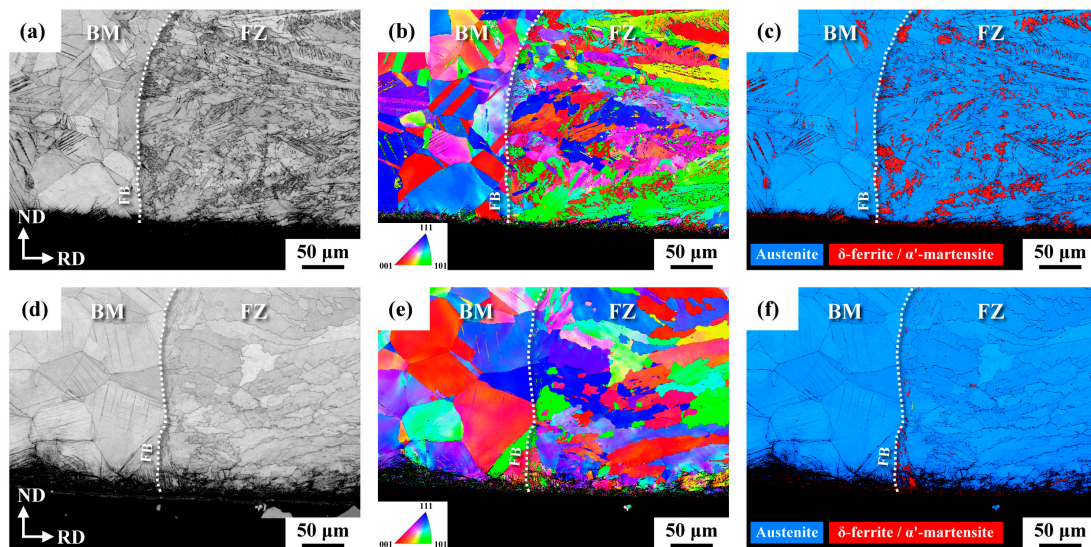


Figure 8. EBSD: (a,d) BC maps, (b,e) IPF maps, (c,f) phase maps of the U-bend samples with micro-shot peening around the FB in cross-sectional view. (a–c) the 304 weld; (d–f) the 316 weld.

3.7. Strain Distribution around the Fusion Boundary of the Welds

As mentioned previously, the strain distribution maps around the FB of the U-bend welds were analyzed by using the HKL Channel 5 software to process the original data obtained by the EBSD and shown in Figures 5 and 6; the results are displayed in Figure 9. As shown in Figure 9a, the zones with intense slip bands and embedded α' -martensite were highly strained regions in the 304 weld. Overall, the FZ exhibited a relatively higher strain than the substrate near the FB. The strain map of the 316 weld (Figure 9b) was similar to that of the 304 weld (Figure 9a), but the strain intensity was lower. It was noticed that the FBs of the welds had higher strain (Figure 9a,b) than the surrounding matrix. The map showing the strain distribution on the top surface around the FB of the U-bend 304 weld (Figure 9c) confirmed the high local strain zones located along the FB and the sites of relatively high intensity of slip bands. Although the strain of the 316 weld was lower than that of the 304 weld (Figure 9d), the FB had high local strain. Therefore, the high concentrated strain at the FB is the most likely cause of the high SCC susceptibility at this site in austenitic SS welds.

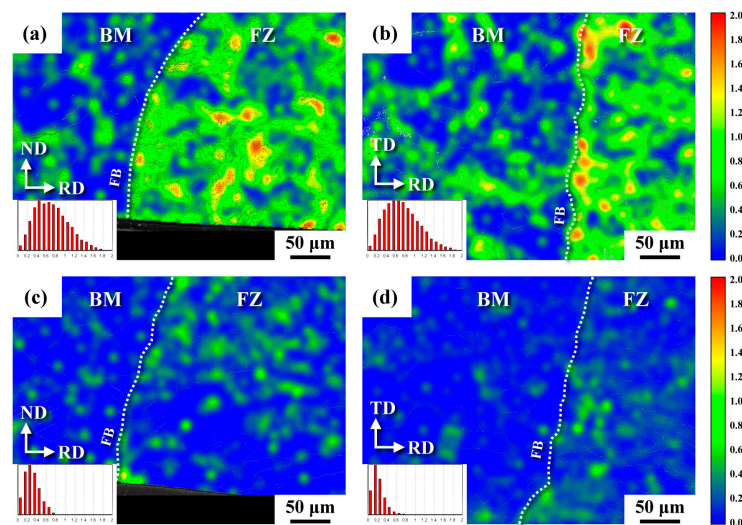


Figure 9. Strain maps around the FB of the (a,b) 304 weld and (c,d) 316 weld. (a,c) cross-sectional views and (b,d) top views.

3.8. The Determinations of Residual Stress of the Welds by XRD

The changes in residual stress in the thickness direction from the external surface to the specific depth of the laser welds in the as-welded and micro-shot peened conditions are shown in Figure 10. In this work, the association between the measured residual stress and the SCC susceptibility of the tested samples was examined. As shown in Figure 10, the residual stresses of the FZs of the 304 and 316 welds were basically in tension. The results indicated that the peak tensile stresses of the as-welded FZs of the two welds were both lower than 150 MPa. The exact reasons for such low tensile stress remain unknown at this time. The low energy input of the laser welding might be the cause of such low residual stress. By contrast, compressive residual stress over -600 MPa was found at the peened surfaces of the two welds. Obviously, the intense micro-shot peening with amorphous powders caused severe plastic deformation and introduced high residual compressive stress to the peened layer. The induced residual compressive stress on the weld surface and weld toe was able to mitigate the adverse effect of residual tensile stress present in the austenitic SS welds.

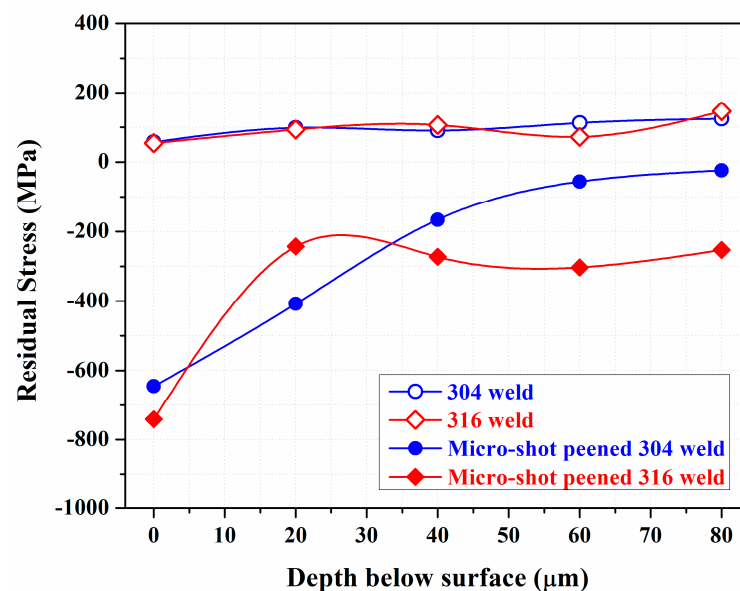


Figure 10. Residual stress distribution of the non-peened and micro-shot peened laser welds determined by XRD.

3.9. Surface Features of the Tested Samples after Salt Spray

In prior work, none of the U-bend samples of the 304 substrate and as-welded 308 WM exhibited visible cracks after exposure to a salt spray for 288 h [36]. Surface damages and microcracks were not observed on the top surface of the U-bend samples before the salt spray tests. The typical surface features of the U-bend samples after the salt spray tests are shown in Figure 11. Without micro-shot peening, observable fine pits were more likely to be found in the FZ, and fine ditches as well as corrosion pits were present at the FB of the welds (Figure 11a). In the non-peened 316 weld, the numbers of visible corrosion pits in the FZ were a little lower than those in the 304 weld (Figure 11b). After micro-shot peening, the 304 weld seemed more susceptible to corrosion, but fine ditches did not appear at the FB of the 304 weld (Figure 11c). Moreover, the formation of corrosion pits and fine ditches was suppressed in the micro-shot peened 316 weld (Figure 11d). Overall, the FB exhibited more continuous corrosion pits and fine ditches than did other zones in the weld, particularly in the non-peened 304 weld.

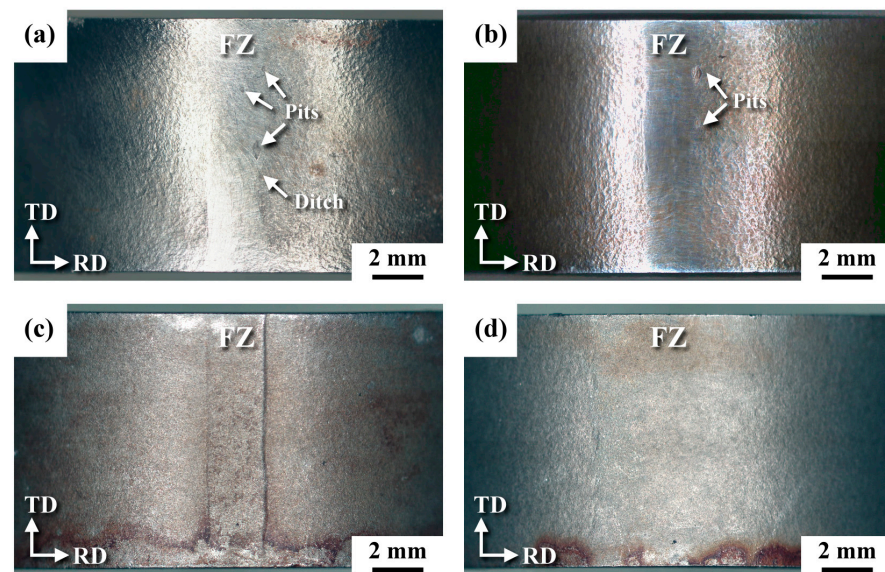


Figure 11. The typical surface morphologies of the U-bend samples after salt spray. (a) 304 weld, (b) 316 weld, (c) micro-shot peened 304 weld and (d) micro-shot peened 316 weld.

The top surface morphology of the U-bend samples after salt spray is inspected with an SEM and the results are displayed in Figure 12. The corroded 304 BM showed mainly intergranular corrosion with transgranular slip lines on the corroded surface (Figure 12a). After micro-shot peening, the corrosion pits of the two SS substrates showed traces of intense slips with microcracks inside the pit (Figure 12b). Overall, the 316 BM exhibited corrosion similar to that of the 304 substrate but with less damage under the same testing condition. The corrosion pits in the FZ of the non-peened 304 weld were similar to those of the 304 BM but larger in size. Regardless of micro-shot peening, the FZ of the 304 weld exhibited numerous corrosion pits, particularly the peened 304 weld (Figure 12c, left). It was noticed that the corrosion pits in the FZ of the peened 304 weld were much finer but greater in number than those in the non-peened 304 weld. Moreover, the bottoms of the pits in the peened FZ were relatively smooth and round in shape (Figure 12c, right). Not only the corrosion pits present in the FZ but also microfissures along the columnar boundaries appeared in the non-peened 304 weld (Figure 12d). As shown in Figure 11, the FBs of the non-peened welds were more likely to be corroded in a salt spray. Coarse pits (Figure 12e) and fine deep cracks (Figure 12f) were also observed at/along the FB of the non-peened 304 and 316 welds. In contrast to the non-peened 316 weld, the micro-shot peened 316 weld showed a relative high resistance to SCC in a salt spray. The peened 316 BM exhibited a dimple surface with very fine microcracks inside (Figure 12g). The micro-appearance around the FB of the peened 316 weld is shown in Figure 12h. The results revealed that the FZ and the HAZ nearby the FB displayed similar morphologies to that of the peened substrate (Figure 12g). It was noticed that the sites around the FB were free of coarse pits and with few microfissures (Figure 12g). Compared with the micro-shot peened 304 weld, the peened FZ and FB of the 316 weld were less damaged after salt spray, possibly due to the inherently high corrosion resistance of the alloy.

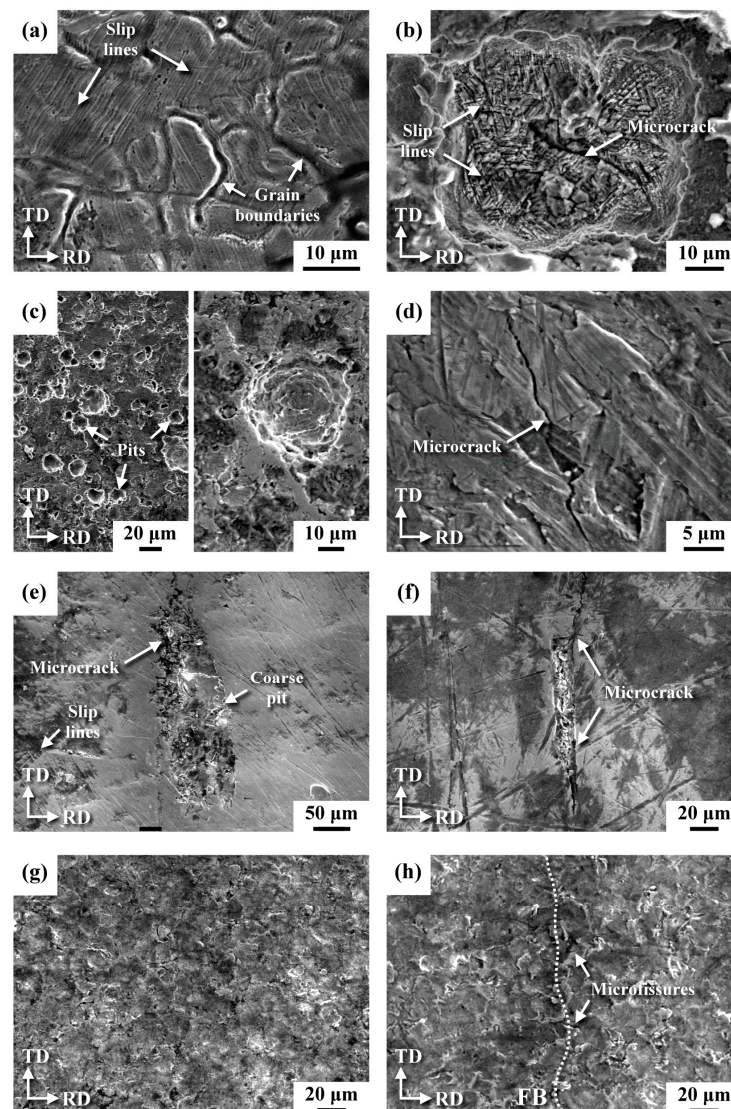


Figure 12. Surface appearance of the U-bend samples after salt spray: (a) 304 BM, (b) micro-shot peened 304 BM, (c) micro-shot peened 304 FZ, (d) microcrack in the FZ of the non-peened 304L weld, (e) corrosion pit at the FB of the non-peened 316 weld, (f) microcrack along the FB of the non-peened 304 weld, (g) micro-shot peened 316 BM, (h) micro-shot peened 316 around the FB.

4. Discussion

The microstructures of the 304 and 316 SSs consisted of granular austenite matrices with twins inside them. Moreover, the microstructure of the 316 FZ was formed predominantly with austenitic cellular dendrites, whereas a skeletal structure having vermicular ferrite (δ ferrite) within the austenite matrix was formed in the FZ of the 304 weld. The SCC of the 304 laser weld in 1 M NaCl + 0.5 M HCl indicated that the preferential dissolution of δ ferrite in the WM results in the SCC growth along the dendrite boundaries [31]. The selective dissolution of the skeletal structure in the 308 WM is the main contributor to the high SCC susceptibility in a salt spray [36]. Therefore, the presence of δ ferrite in the FZ of a 304 laser weld would decrease its SCC resistance in a salt spray.

Under the same bending strain, slips occur more easily in the 304 FZ than in the 316 one, i.e., the 304 weld was less resistant than the 316 weld to dislocation motions. Therefore, a higher amount of α' -martensite formed in the former than in the latter. Microvoids are more likely to form at the slip bands [36] and the preferential dissolution occurs in the area with intense slip bands in a salt spray [36], which is associated with the formation of α' -martensite.

Therefore, the presence of δ ferrite, as well as the greater extent of α' -martensite formed on the top surface of a U-bend 304 FZ, would naturally be sensitive to SCC in a salt spray.

The strain distribution maps around the FB of the U-bend welds were analyzed by EBSD and are shown in Figure 9. Those regions with intense slip bands and embedded α' -martensite in the 304 weld had high strain. This may have been due to the low amount of dislocation motion, explaining the lower strain intensity in the 316 weld relative to that in the 304 weld, although both welds were subjected to the same bending strain (Figure 9a,b). High concentrated strain was located along the FBs of the two welds (Figure 9). Thus, the FBs of the two austenitic welds would be susceptible to SCC in a salt spray. The surface features of the damaged 304 and 316 laser welds in a salt spray confirmed the ease of pitting and cracking along the FBs of the welds (Figures 11 and 12).

It is reported that ultrasonic peening can effectively improve the SCC resistance of 304 welds in boiling 42% MgCl solution [37]. In this study, a nanocrystalline structure was formed (Figure 7) and residual compressive stress was introduced (Figure 10) in the micro-shot peened layer. Extensive formation of α' -martensite was detrimental to the corrosion resistance of micro-shot peened samples in a salt spray. In a 304 weld under a slow strain rate tensile test in 3.5% NaCl solution, the grain refinement causes a decrease in the stress corrosion sensitivity index, but the extensive formation of martensite on the shot peened 304 weld is harmful to the SCC resistance [38]. It was obvious that micro-shot peening would assist the formation of α' -martensite, which could reduce the pitting resistance. However, the nanocrystalline structure and residual compressive stress could suppress the occurrence of SCC of the U-bend welds in a salt spray. The high local strain or high residual tensile stress at the FBs of the welds could be reversed by micro-shot peening, and the crack initiation thereby impeded. Moreover, geometrical modification of the weld toe and the introduction of residual compressive stress into a 304 weld by ultrasonic peening improves the fatigue life and provides corrosion resistance as good as or even better than the BM [39]. It was deduced that micro-shot peening could be an effective process to mitigate the SCC susceptibility of the austenitic SS welds.

5. Conclusions

1. Under the same bending strain, the FZs of the austenitic SS welds showed higher strain hardening and martensitic transformation than the other zones in the laser welds, especially in the 304 FZ. The lower number of slip bands in the 316 weld than in the 304 weld implied a higher resistance to dislocation motions in the former than in the latter, resulting in forming smaller amounts of α' -martensite in the former. The preferential dissolution of α' -martensite and δ ferrite in the FZ of a 304 weld was detrimental to the pitting corrosion and SCC resistance in a salt spray.
2. The strain distribution maps around the FB of the U-bend welds showed that the regions in the 304 weld with intense slip bands and embedded α' -martensite had high local strain. In addition, the 316 weld showed a low strain intensity relative to that of the 304 weld under the same bending strain. High local strain along the FBs of the two welds was observed, especially in the 304 weld. The surface features of the corroded 304 and 316 welds confirmed the ease of pitting and cracking along the FBs in a salt spray.
3. Micro-shot peening resulted in the formation of a nanograined structure, induced martensite and introduced residual compressive stress in the severe micro-shot peened layer. Extensive formation of α' -martensite was harmful to the pitting resistance of the austenitic SSs in a salt spray. The coarse pits and microfissures that formed in the non-peened 304 FZ were replaced by numerous fine pits in the peened 304 FZ. The high local strain at the FB was the cause of the high pitting and cracking susceptibility relative to other zones in the austenitic SS weld in a salt spray. The fine-grained structure and imposed residual compressive stress suppressed the microcrack initiation at the FB of the 304 and 316 laser welds in a salt spray.

Author Contributions: Conceptualization, L.-W.T.; methodology, L.-W.T.; formal analysis, C.-Y.K. and T.-C.C.; investigation, C.-Y.K. and T.-C.C.; resources, L.-W.T.; writing—original draft preparation, L.-W.T.; writing—review and editing, T.-C.C.; visualization, T.-C.C.; supervision, L.-W.T.; project administration, L.-W.T.; funding acquisition, L.-W.T. All authors have read and agreed to the published version of the manuscript.

Funding: This research was funded by the Ministry of Science and Technology, R.O.C., grant number MOST 109-2221-E-019-023-MY3.

Data Availability Statement: Data available on request due to restrictions, e.g., privacy or ethical.

Acknowledgments: The authors are grateful to the Ministry of Science and Technology for the support. The authors are grateful to the Core Facility Center of National Cheng Kung University (OTHER002200) for granting access to the 3D optical profiler. The authors would also like to thank Likuan Technology Corp. for their great help in determining the residual stress of the micro-shot peened samples and Vincent Vacuum Tech. for performing the micro-shot peening.

Conflicts of Interest: The authors declare no conflict of interest.

Abbreviations

SS	stainless steel
SCC	stress corrosion cracking
WM	weld metal
HAZ	heat-affected zone
SEM	scanning electron microscope
EBS	electron backscatter diffraction
ND	normal direction
RD	rolling direction
TD	transverse direction
FN	ferrite number
FZ	fusion zone
BM	base metal
FB	fusion boundary
BC	band contrast
IPF	inverse pole figure

References

1. Bagherifard, S.; Slawik, S.; Fernández-Pariente, I.; Pauly, C.; Mücklich, F.; Guagliano, M. Nanoscale surface modification of AISI 316L stainless steel by severe shot peening. *Mater. Des.* **2016**, *10*, 68–77. [\[CrossRef\]](#)
2. Jayalakshmi, M.; Huilgol, P.; Bhat, B.R.; Udaya Bhat, K. Insights into formation of gradient nanostructured (GNS) layer and deformation induced martensite in AISI 316 stainless steel subjected to severe shot peening. *Surf. Coat. Technol.* **2018**, *344*, 295–302. [\[CrossRef\]](#)
3. Unal, O.; Varol, R. Surface severe plastic deformation of AISI 304 via conventional shot peening, severe shot peening and reopening. *Appl. Surf. Sci.* **2015**, *351*, 289–295. [\[CrossRef\]](#)
4. He, Y.; Lee, H.S.; Yang, C.W.; Lee, J.H.; Shin, K. Microstructural Evolution of A Nanostructure of Shot Peened 304 Stainless Steel Upon Heat Treatment. *Sci. Adv. Mater.* **2017**, *9*, 1942–1946. [\[CrossRef\]](#)
5. Ni, Z.; Wang, X.; Wang, J.; Wu, E. Characterization of the phase transformation in a nanostructured surface layer of 304 stainless steel induced by high-energy shot peening. *Phys. B Condens. Matter* **2003**, *334*, 221–228. [\[CrossRef\]](#)
6. Yu, H.; Dong, J.L.; Yoo, D.H.; Shin, K.; Jung, J.S.; Pyoun, Y.; Cho, I. Effect of Ultrasonic and Air Blast Shot Peening on the Microstructural Evolution and Mechanical Properties of SUS304. *J. Korean Phys. Soc.* **2009**, *54*, 1161–1166. [\[CrossRef\]](#)
7. Han, X.; Zhang, Z.; Hou, J.; Barber, G.C.; Qin, F. Tribological behavior of shot peened/austempered AISI 5160 steel. *Tribol. Int.* **2020**, *145*, 106197. [\[CrossRef\]](#)
8. Zhan, K.; Zhang, Y.; Zhao, S.; Yang, Z.; Zhao, B.; Ji, V. Tribological Behavior and Corrosion Resistance of S30432 Steel after Different Shot Peening Processes. *J. Mater. Eng. Perform.* **2022**, *31*, 1250–1258. [\[CrossRef\]](#)
9. Bagherifard, S.; Hickey, D.J.; Luca, A.C.; Malheiro, V.N.; Markaki, A.E.; Guagliano, M.; Webster, T.J. The influence of nanostructured features on bacterial adhesion and bone cell functions on severely shot peened 316L stainless steel. *Biomaterials* **2015**, *73*, 185–197. [\[CrossRef\]](#)
10. Kumar, N.; Chaudhari, G.P.; Meka, S.R. Influence of Ultrasonic Shot Peening on Microstructure, Mechanical, and Electrochemical Behavior of 316 Stainless Steel. *J. Mater. Eng. Perform.* **2021**, *31*, 2364–2380. [\[CrossRef\]](#)
11. Suh, M.-S.; Suh, C.-M.; Pyun, Y.-S. Very high cycle fatigue characteristics of a chrome-molybdenum steel treated by ultrasonic nanocrystal surface modification technique. *Fatigue Fract. Eng. Mater. Struct.* **2013**, *36*, 769–778. [\[CrossRef\]](#)

12. Sledz, M.; Stachowicz, F.; Zielecki, W. The effect of shot peening on the fatigue strength of steel sheets. *Kov. Mater.–Met. Mater.* **2015**, *53*, 91–95. [\[CrossRef\]](#)
13. Khan, M.K.; Fitzpatrick, M.E.; Wang, Q.Y.; Pyoun, Y.S.; Amanov, A. Effect of ultrasonic nanocrystal surface modification on residual stress and fatigue cracking in engineering alloys. *Fatigue Fract. Eng. Mater. Struct.* **2017**, *41*, 844–855. [\[CrossRef\]](#)
14. Segurado, E.; Belzunce, J.; Fernández, I. Enhanced Fatigue Behavior in Quenched and Tempered High-Strength Steel by Means of Double Surface Treatments. *J. Mater. Eng. Perform.* **2019**, *28*, 2094–2102. [\[CrossRef\]](#)
15. Masaki, K.; Ochi, Y.; Matsumura, T. Initiation and propagation behaviour of fatigue cracks in hard-shot peened Type 316L steel in high cycle fatigue. *Fatigue Fract. Eng. Mater. Struct.* **2004**, *27*, 1137–1145. [\[CrossRef\]](#)
16. Sano, Y.; Obata, M.; Kubo, T.; Mukai, N.; Yoda, M.; Masaki, K.; Ochi, Y. Retardation of crack initiation and growth in austenitic stainless steels by laser peening without protective coating. *Mater. Sci. Eng. A* **2006**, *417*, 334–340. [\[CrossRef\]](#)
17. Amanov, A.; Karimbaev, R.; Maleki, E.; Unal, O.; Pyun, Y.-S.; Amanov, T. Effect of combined shot peening and ultrasonic nanocrystal surface modification processes on the fatigue performance of AISI 304. *Surf. Coat. Technol.* **2019**, *358*, 695–705. [\[CrossRef\]](#)
18. Odnobokova, M.; Belyakov, A.; Enikeev, N.; Kaibyshev, R.; Valiev, R.Z. Microstructural changes and strengthening of austenitic stainless steels during rolling at 473 K. *Metals* **2020**, *10*, 1614. [\[CrossRef\]](#)
19. Droste, M.; Henkel, S.; Biermann, H.; Weidner, A. Influence of plastic strain control on martensite evolution and fatigue life of metastable austenitic stainless steel. *Metals* **2022**, *12*, 1222. [\[CrossRef\]](#)
20. Yu, C.; Shiue, R.-K.; Chen, C.; Tsay, L.-W. Effect of low-temperature sensitization on hydrogen embrittlement of 301 stainless steel. *Metals* **2017**, *7*, 58. [\[CrossRef\]](#)
21. Chung, Y.-H.; Chen, T.-C.; Lee, H.-B.; Tsay, L.-W. Effect of Micro-Shot Peening on the Fatigue Performance of AISI 304 Stainless Steel. *Metals* **2021**, *11*, 1408. [\[CrossRef\]](#)
22. Kikuchi, S.; Nakamura, Y.; Nambu, K.; Ando, M. Effect of Shot Peening Using Ultra-Fine Particles on Fatigue Properties of 5056 Aluminum Alloy under Rotating Bending. *Mater. Sci. Eng. A* **2016**, *652*, 279–286. [\[CrossRef\]](#)
23. Lee, H.-S.; Kim, D.-S.; Jung, J.-S.; Pyoun, Y.-S.; Shin, K. Influence of peening on the corrosion properties of AISI 304 stainless steel. *Corros. Sci.* **2009**, *51*, 2826–2830. [\[CrossRef\]](#)
24. Wei, X.; Zhu, D.; Ling, Y.; Dai, M. Influence of Wet Micro-Shot Peening on Surface Properties and Corrosion Resistance of AISI 304 Stainless Steel. *Int. J. Electrochem. Sci.* **2018**, *13*, 4198–4207. [\[CrossRef\]](#)
25. Chen, X.; Li, Y.; Zhu, Y.; Bai, Y.; Yang, B. Improved corrosion resistance of 316LN stainless steel performed by rotationally accelerated shot peening. *Appl. Surf. Sci.* **2019**, *481*, 1305–1312. [\[CrossRef\]](#)
26. Okido, S.; Yoshimura, T.; Enomoto, K.; Saito, H.; Morinaka, R.; Ishikawa, T. Preventive Effect of Shot Peening on Stress Corrosion Cracking. *Mater. Sci. Res. Int.* **2002**, *8*, 193–198. [\[CrossRef\]](#)
27. Naito, A.; Takakuwa, O.; Soyama, H. Development of peening technique using recirculating shot accelerated by water jet. *Mater. Sci. Technol.* **2012**, *28*, 234–239. [\[CrossRef\]](#)
28. Park, I.; Kim, E.-Y.; Yang, W. Microstructural Investigation of Stress Corrosion Cracking in Cold-Formed AISI 304 Reactor. *Metals* **2021**, *11*, 7. [\[CrossRef\]](#)
29. Sreevidya, N.; Abhijith, S.; Albert, S.K.; Vinod, V.; Banerjee, I. Failure analysis of service exposed austenitic stainless steel pipelines. *Eng. Fail. Anal.* **2020**, *108*, 104337. [\[CrossRef\]](#)
30. Luo, Y.; Gu, W.; Wei, P.; Jin, Q.; Qin, Q.; Yi, C. A Study on Microstructure, Residual Stresses and Stress Corrosion Cracking of Repair Welding on 304 Stainless Steel: Part I-Effects of Heat Input. *Materials* **2020**, *13*, 2416. [\[CrossRef\]](#)
31. Lu, B.-T.; Chen, Z.-K.; Luo, J.-L.; Patchett, B.M.; Xu, Z.-H. Stress corrosion crack initiation and propagation in longitudinally welded 304 austenitic stainless steel. *Corros. Eng. Sci. Technol.* **2003**, *38*, 69–75. [\[CrossRef\]](#)
32. Lu, J.; Hultman, L.; Holmström, E.; Antonsson, K.H.; Grehk, M.; Li, W.; Vitos, L.; Golpayegani, A. Stacking fault energies in austenitic stainless steels. *Acta Mater.* **2016**, *111*, 39–46. [\[CrossRef\]](#)
33. Wang, X.; Xiong, W. Stacking fault energy prediction for austenitic steels: Thermodynamic modeling vs. machine learning. *Eng. Struct. Mater.* **2020**, *21*, 626–634. [\[CrossRef\]](#) [\[PubMed\]](#)
34. Román, A.; Campillo, B.; Martínez, H.; Flores, O. Prediction of the stacking fault energy in austenitic stainless steels using an artificial neural network. *Int. J. Eng. Tech. Res.* **2019**, *9*, 31–38. [\[CrossRef\]](#)
35. Hadji, M.; Badji, R. Microstructure and Mechanical Properties of Austenitic Stainless Steels After Cold Rolling. *J. Mater. Eng. Perform.* **2002**, *11*, 145–151. [\[CrossRef\]](#)
36. Hsu, C.-H.; Chen, T.-C.; Huang, R.-T.; Tsay, L.-W. Stress Corrosion Cracking Susceptibility of 304L Substrate and 308L Weld Metal Exposed to a Salt Spray. *Materials* **2017**, *10*, 187. [\[CrossRef\]](#)
37. Ling, X.; Ma, G. Effect of ultrasonic impact treatment on the stress corrosion cracking of 304 stainless steel welded joints. *J. Press. Vessel. Technol. ASME* **2009**, *131*, 051502. [\[CrossRef\]](#)
38. Lu, Z.; Shi, L.; Zhu, S.; Tang, Z.; Jiang, Y. Effect of high energy shot peening pressure on the stress corrosion cracking of the weld joint of 304 austenitic stainless steel. *Mater. Sci. Eng. A* **2015**, *637*, 170–174.
39. Abdullah, A.; Malaki, M.; Eskandari, A. Strength enhancement of the welded structures by ultrasonic peening. *Mater. Des.* **2012**, *38*, 7–18.

Disclaimer/Publisher’s Note: The statements, opinions and data contained in all publications are solely those of the individual author(s) and contributor(s) and not of MDPI and/or the editor(s). MDPI and/or the editor(s) disclaim responsibility for any injury to people or property resulting from any ideas, methods, instructions or products referred to in the content.